ENVIRONMENTAL RESEARCH
LETTERS

PAPER • OPEN ACCESS

Warm-season net CO_2 uptake outweighs cold-season emissions over Alaskan North Slope tundra under current and RCP8.5 climate

IOP Publishing Environ. Res. Lett. 16 (2021) 055012 https://doi.org/10.1088/1748-9326/abf6f5

ENVIRONMENTAL RESEARCH
LETTERS

OPEN ACCESS

RECEIVED
16 November 2020

REVISED
16 March 2021

ACCEPTED FOR PUBLICATION
12 April 2021

PUBLISHED
30 April 2021

LETTER

Warm-season net CO_2 uptake outweighs cold-season emissions over Alaskan North Slope tundra under current and RCP8.5 climate

Jing Tao[1,2,*], **Qing Zhu**[1], **William J Riley**[1] **and Rebecca B Neumann**[2]

[1] Climate and Ecosystem Sciences Division, Lawrence Berkeley National Laboratory, Berkeley, CA, United States of America
[2] Department of Civil and Environmental Engineering, University of Washington, Seattle, WA, United States of America
[*] Author to whom any correspondence should be addressed.

E-mail: JingTao@lbl.gov

Keywords: soil respiration, carbon budget, Alaskan Arctic tundra, tundra plant resilience, hydroclimatic extremes, E3SM land model (ELM)

Supplementary material for this article is available online

Abstract

Arctic warming has increased vegetation growth and soil respiration during recent decades. The rate of Arctic warming will likely amplify over the 21st century. Previous studies have revealed that the most severe Arctic warming occurred during the cold season (September to May). The cold-season warming has posited significant CO_2 emissions to the atmosphere via respiration, possibly offsetting warm-season (June to August) net CO_2 uptake. However, prevailing Earth system land models poorly represent cold-season CO_2 emissions, making estimates of Arctic tundra annual CO_2 budgets highly uncertain. Here, we demonstrate that an improved version of the energy exascale Earth system model (E3SM) land model (ELMv1-ECA) captures the large amount of cold-season CO_2 emissions over Alaskan Arctic tundra as reported by two independent, observationally-constrained datasets. We found that the recent seven-decades warming trend of cold-season soil temperature is three times that of the warm-season. The climate sensitivity of warm-season net CO_2 uptake, however, is threefold higher than for the cold-season net CO_2 loss, mainly due to stronger plant resilience than microbial resilience to hydroclimatic extremes. Consequently, the modeled warm-season net CO_2 uptake has a larger positive trend (0.74 ± 0.14 gC m^{-2} yr^{-1}) than that of cold-season CO_2 emissions (0.64 ± 0.11 gC m^{-2} yr^{-1}) from 1950 to 2017, supported by enhanced plant nutrient uptake and increased light- and water-use efficiency. With continued warming and elevated CO_2 concentrations under the representative concentration pathway (RCP) 8.5 scenario, the increasing rate of warm-season net CO_2 uptake is more than twice the rate of cold-season emissions (1.33 ± 0.32 gC m^{-2} yr^{-1} vs 0.50 ± 0.12 gC m^{-2} yr^{-1}), making the modeled Alaskan Arctic tundra ecosystem a net CO_2 sink by 2100. However, other geomorphological and ecological disturbances (e.g. abrupt permafrost thaw, thermokarst development, landscape-scale hydrological changes, wildfire, and insects) that are not considered here might alter our conclusion.

1. Introduction

Permafrost regions have undergone persistent warming during recent decades (Pithan and Mauritsen 2014, Huang *et al* 2017, Biskaborn *et al* 2019), and the Arctic tundra ecosystem has warmed more than any other biome (Bjorkman *et al* 2018). This warming, and likely the CO_2 fertilization effects, has increased ecosystem photosynthesis, productivity, and widespread expansion of tall shrubs in the Arctic tundra, leading to enhanced growing-season carbon uptake (Elmendorf *et al* 2012, Frost *et al* 2013, Zhang *et al* 2013, Martin *et al* 2017, Mekonnen *et al* 2018a, Berner *et al* 2020, Wang *et al* 2020). Meanwhile,

permafrost thaw has made the organic carbon and nitrogen previously locked in permafrost soils available to microbial decomposition (Lawrence *et al* 2008, Koven *et al* 2011, Hugelius *et al* 2014, Mishra and Riley 2014, Schaefer *et al* 2014), thereby increasing both plant growth and ecosystem respiration (Waelbroeck *et al* 1997, McGuire *et al* 2012, Natali *et al* 2012, Trucco *et al* 2012, Koven *et al* 2015, Schuur *et al* 2015, Parazoo *et al* 2018, Mekonnen *et al* 2018a, Gagnon *et al* 2019). The most severe Arctic warming has occurred during the cold season (Sturm *et al* 2005, Koenigk *et al* 2013, Cohen *et al* 2014, 2018, Huang *et al* 2017, Box *et al* 2019), which increases microbial decomposition of soil organic matter and thus enhances cold-season soil heterotrophic respiration (HR), releasing a significant amount of carbon via methane (CH_4) and carbon dioxide (CO_2) (Zona *et al* 2016, Natali *et al* 2019). Cold-season CO_2 emissions might largely offset the warm-season CO_2 net uptake, and become increasingly important in annual carbon budgets over Arctic tundra ecosystems (Commane *et al* 2017b, Jeong *et al* 2018, Campbell and Laudon 2019, Natali *et al* 2019).

Site-scale measurements have demonstrated large cold-season CO_2 losses over the pan-Arctic tundra ecosystem (e.g. Fahnestock *et al* 1998, Jones *et al* 1999, Kittler *et al* 2017). Some studies indicated that with warming, cold-season CO_2 emissions from the Alaskan Arctic tundra grew larger than summer net uptake, i.e. shifted from an annual sink to an annual source of CO_2 (Oechel *et al* 1993, 2000, 2014). Belshe *et al* (2013) also concluded that tundra sites were annual sources of CO_2 from the mid-1980s until the 2000s. Despite these conclusions at the site scale, long-term regional estimates of cold-season CO_2 emissions remain uncertain due to limited spatial representativeness of site-scale observations (Rustad *et al* 2001, McGuire *et al* 2012) and the lack of continuous measurements throughout the entire cold season (Oechel *et al* 1993, McGuire *et al* 2012, Parazoo *et al* 2016).

Process-based terrestrial ecosystem models can facilitate the estimate of long-term, regional cold-season CO_2 budgets. However, most current land models integrated within Earth system models (ESMs) poorly represent cold-season carbon emissions (Zona *et al* 2016, Commane *et al* 2017b, Wang *et al* 2019, Natali *et al* 2019), making estimations and predictions of regional net ecosystem exchanges (NEE) of CO_2 over the Arctic tundra highly uncertain (McGuire *et al* 2012, Fisher *et al* 2014). The coupled model intercomparison project 5 (CMIP5) models, for instance, substantially underestimated early winter respiration rates over Alaska (Commane *et al* 2017b), partially due to inadequately represented zero-curtain periods (ZCP) (i.e. the period when soil temperatures linger around 0 °C during the freezing season) (Outcalt *et al* 1990). With a warming climate, the ZCP duration over the Arctic tundra is expected to increase (Zona *et al* 2016, Arndt *et al* 2019). However, different representations of ZCP and cold-season soil respirations over Arctic tundra might lead to contradictory conclusions on the annual CO_2 budget among models. For instance, Zhang *et al* (2014) predicted that under the representative concentration pathway (RCP) 8.5 scenario, the Arctic tundra will remain a carbon sink throughout the 21st century due to enhanced biogeophysical feedbacks. Similar conclusions were found by many other studies (e.g. Qian *et al* 2010, Zhang *et al* 2013, Mekonnen *et al* 2018a). Other modeling studies, in contrast, have concluded that cold-season carbon emissions might eventually offset summer net carbon uptake under 21st century warming climate, potentially transforming permafrost tundra ecosystems from a net sink to a net source of carbon (e.g. Piao *et al* 2008). Without close examination of the representation of ZCP and cold-season carbon emissions, it is hard to quantify the annual CO_2 budget with high confidence.

Relying on site-scale observations, Natali *et al* (2019) derived winter-time CO_2 emissions over high-latitude permafrost regions with a machine learning approach, and reported that 1662 TgC yr^{-1} were lost via CO_2 from their domain from October to April between 2003 and 2017. By combining the machine-learning cold-season CO_2 emission estimates and independent multiple-model estimates of warm-season net CO_2 uptake, they further concluded that the current permafrost region is a net annual CO_2 source with annual emissions ranging from 15 to 975 TgC yr^{-1}, and that, under a continued warming climate, increases in cold-season CO_2 emissions might exceed increases in warm-season net uptake. However, large uncertainties exist in the predicted future emissions because the data-driven model trained by current *in-situ* measurements might not be able to capture future ecosystem responses to a changing climate (Natali *et al* 2019). Therefore, reasonably representing the ZCP and overall cold-season carbon processes within process-based land models is urgently needed to better predict carbon budgets of Arctic tundra ecosystems (Commane *et al* 2017b, Campbell and Laudon 2019).

Recently, relying on observations from the Arctic-boreal vulnerability experiment (ABoVE) and the carbon in Arctic reservoirs vulnerability experiment (CARVE), Tao *et al* (2020) improved the energy exascale Earth system model (E3SM) land model (ELMv1-ECA) in terms of simulating ZCPs and cold-season CO_2 emissions at several Alaska tundra sites (figure 1). Here we adopted the updated ELMv1-ECA to address the long-standing question of whether cold-season CO_2 emissions offset the warm-season

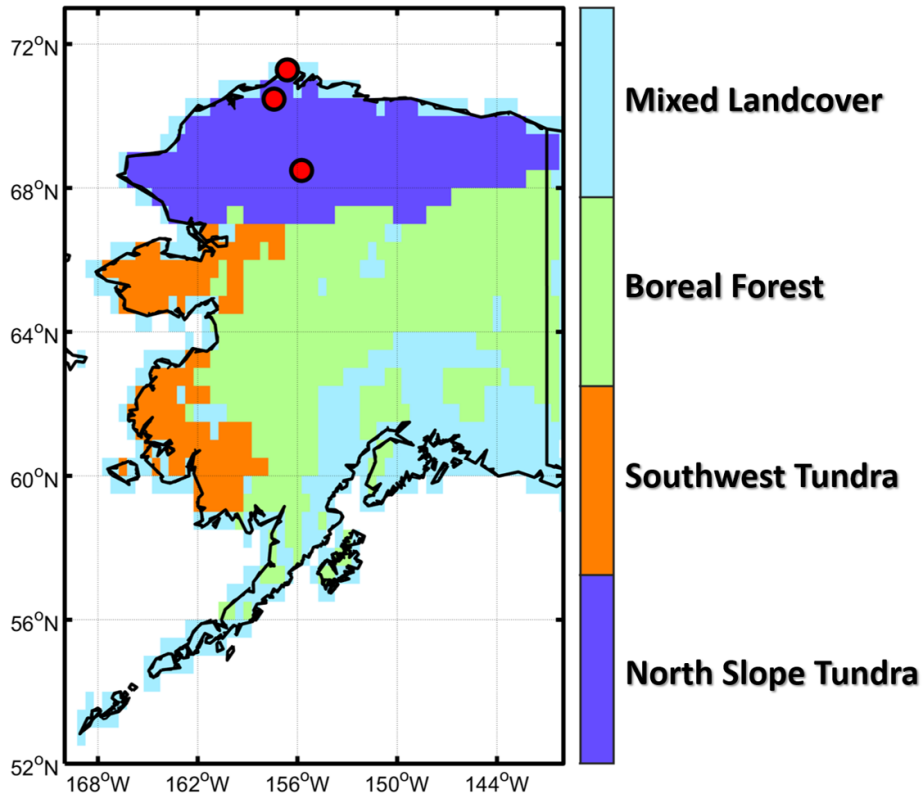

Figure 1. Landcover map of Alaska (adapted from Commane *et al* 2017a). Each pixel color indicates the land cover type covering more than 50% of the grid cell area. Red dots indicate ABoVE flux tower sites studied in Tao *et al* (2020).

net uptake over the Alaskan North Slope tundra (NST) currently and over the 21st century.

2. Methodology

2.1. Study domain and data

We mainly focused on the Alaskan NST (figure 1), adopting the landcover map in Commane *et al* (2017b). We also examined results over the interior boreal forest (BF) and Southwest tundra (SWT) areas in supplementary section sup. 2 (available online at stacks.iop.org/ERL/16/055012/mmedia). We used two independent observationally-constrained spatial datasets to evaluate model results. Details about the two datasets and processing methodology are provided in the supplementary section sup. 1.

First, we used a spatial NEE dataset optimized with CARVE aircraft measurements (Commane *et al* 2017a, 2017b) as a benchmark to evaluate the regional simulation results over Alaska from 2012 to 2014. The CARVE airborne measurements span April through November, and thus the optimized NEE are only available over these months (supplementary figure S1)[3]. Hereafter, we use '*C2017*' to represent this observation-constrained, aircraft-optimized spatial NEE dataset.

[3] Figures numbered with a prefix 'S' are include in the supplementary file.

We also used another observation-constrained spatial dataset of cold-season CO_2 emissions derived from ground flux observations with a boosted regression tree machine learning method (Watts *et al* 2019, Natali *et al* 2019). We denote this observation-constrained dataset as '*N2019*'. The *N2019* includes spatially-resolved September to April CO_2 emissions over northern permafrost regions from 2003 to 2017, and predicted cold-season CO_2 emissions from 2018 to 2100 using their method and CMIP5 outputs under the RCP8.5 scenario.

2.2. Model and experiment design

The ELMv1-ECA simulates terrestrial carbon cycles, energy, and water exchange fluxes, and accounts for the limitation of nutrient availability for plant growth (Riley *et al* 2018, Chen *et al* 2019, Golaz *et al* 2019, Zhu *et al* 2019, 2020). Here, we used the version of ELMv1-ECA updated by Tao *et al* (2020), denoted as ELMv1a hereafter. ELMv1a differs from ELMv1-ECA mainly in its phase-change scheme and soil organic carbon decomposition scheme, and cold-season methane transport mechanism. We have calibrated and evaluated the ELMv1a against eddy covariance observations at Alaska tundra sites (figure 1) (Tao *et al* 2020). Compared to ELMv1-ECA, ELMv1a has shown enhanced performance in simulated ZCPs of active-layer soils and cold-season CO_2 and emissions at the site scale. At the regional scale over the NST, we identified a generic decomposition

scheme which uses a Q_{10} value of 2.0 and a modified moisture-dependency function that prevents zero respiration in freezing and subfreezing soils (Tao *et al* 2020).

With ELMv1a, we conducted a transient simulation from 1901 to 2017 at 30 min temporal resolution over Alaska, driven by 0.5° × 0.5° climatic research unit Japanese reanalysis (CRU JRA) climate forcing (Harris 2019). The transient simulation started from properly spun-up simulations following Zhu *et al* (2019). We estimated model uncertainty associated with representations of temperature sensitivity to HR through simulations with a range of Q_{10} values (1.6–2.2) (Tao *et al* 2020). We then ran three future simulations through 2100 under the RCP8.5 scenario (Friedlingstein *et al* 2006), including (a) with RCP8.5 climate forcing but CO_2 concentration fixed at 2011 levels (denoted as RCP8.5_climate), (b) with evolving elevated CO_2 concentration but repeatedly cycling 2011–2020 climate forcing (denoted as RCP8.5_eCO_2), and (c) with both predicted RCP8.5 climate and evolving CO_2 concentration (denoted as RCP8.5_climate + eCO_2). Then, we characterize the trends of warm-season net CO_2 uptake and cold-season CO_2 loss over the Alaskan NST and the whole Alaska domain.

Studies have shown that net primary productivity (NPP) enhancement resulting from elevated CO_2 might be attenuated by limited nutrient availability (Norby *et al* 2010, Zaehle *et al* 2014, Wang *et al* 2020). We thus disentangled the integrated ecosystem response into major nitrogen (N) and phosphorus (P) cycling processes, including plant N and P uptake, net N and P mineralization, N and P limitation, N- and P-use efficiency (NUE and PUE). We also examined water- and light-use efficiency (WUE and LUE). Details about these subcomponent processes are provided in the supplementary sup. 4.

We defined 'warm season' as June to August and 'cold season' as September to May. We further defined an early cold season period from September through October. We estimated the NEE trend for each period as the regression slope between annual or seasonal NEE and time. The computed trend is statistically significant if the *p*-value is less than 0.05. Further, similar to Ballantyne *et al* (2017), we calculated and discussed the climate sensitivity of warm-season total net CO_2 uptake and cold-season total net CO_2 emissions (supplementary sup. 3).

3. Results and discussion

3.1. Evaluation of simulated NEE

We evaluated simulated NEE against the two spatial datasets (i.e. *C2017* and *N2019*) at both pixel and regional scales. We used *C2017* to evaluate results during the warm season and at the annual scale from 2012 to 2014. We also compared results with both *N2019* and *C2017* over their common period (i.e. 2012–2014). Then, we compared simulated cold-season CO_2 emissions against *N2019* throughout 2003–2017.

Pixel-scale RMSE of ELMv1a-simulated monthly NEE (figure 2(b)) varied between 0.3 and 3.7 gC m^{-2} d^{-1} for the warm season and between 0.2 and 1.4 gC m^{-2} d^{-1} for the cold season (compared to *C2017*). There were large spatial patterns in the NEE RMSE, with the largest cold-season RMSE values clustering in the interior BF regions and largest warm-season values scattering across Alaska (figure 2(b)). Reasons potentially contributing to higher NEE RMSE include inaccurate forcing and landscape parameters prescribed and model deficiencies, as summarized at the end of this section. Compared to ELMv1-ECA (figure 2(a)), ELMv1a improved simulated cold-season CO_2 emissions at the pixel scale, especially over the NST. The RMSE (compared with *C2017*) of ELMv1a-simulated regional mean NEE over the NST was reduced from 0.43 gC m^{-2} d^{-1} to 0.39 gC m^{-2} d^{-1} (figure S2). Evaluating against the *N2019* CO_2 emissions over September to April, ELMv1a showed a significantly improved performance over ELMv1-ECA, with a 55% reduction in RMSE (0.14 vs 0.31 gC m^{-2} d^{-1}) (figure S2). We, therefore, apply ELMv1a-simulated results for the remaining analyses.

ELMv1a overestimated warm-season CO_2 net uptake compared to *C2017* (figure 3) by 0.23 gC m^{-2} d^{-1} (31%) and 0.44 gC m^{-2} d^{-1} (44%) on average for NST and the whole Alaska domain, respectively. Shoulder-season (i.e. September, October, and May) CO_2 release was underestimated compared to *C2017* but not compared to *N2019*. The ELMv1a-simulated regional means agreed well with *C2017* over the rest of the cold-season months for the NST and SWT regions, with slight overestimations for cold-season emissions over the BF region (figure 3). Compared to *N2019*, results demonstrate very good performance for all the major landcover types and entire Alaska. Because of a lack of cold-season aircraft measurements (figure 3) for *C2017*, we relied on *N2019* for this comparison. Specifically, results show the best performance for the regional mean over entire Alaska with the smallest RMSE of 0.08 gC m^{-2} d^{-1}, followed by the RMSE of 0.14 gC m^{-2} d^{-1} for tundra ecosystems (table S1).

The ELMv1a simulated 2012–2014 averaged cold-season total CO_2 emissions over the NST show biases within 30% of the observed values, i.e. 24.7 gC m^{-2} yr^{-1} (24%) compared to *N2019* and 31.9 gC m^{-2} yr^{-1} (29%) compared to *C2017* (figure 4(a)). For the early cold season (September to October), when the ZCP of the active layer in Arctic tundra is most often present, the model simulated total CO_2 emissions match very well with *N2019*, with biases of 8.2 gC m^{-2} yr^{-1} (21%) for NST and 0.9 gC m^{-2} yr^{-1} (2%) for Alaska. The annual total NEE (positive) from *C2017* indicates

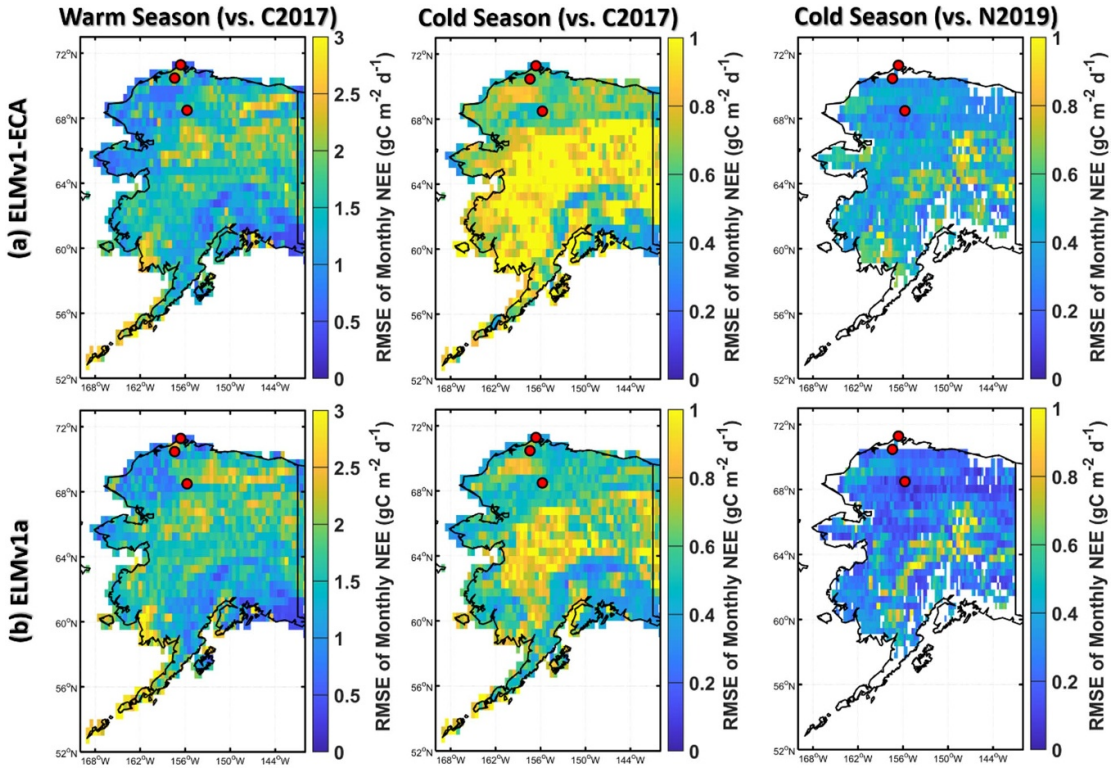

Figure 2. Pixel-scale RMSE of ELM-simulated monthly NEE against *C2017* over the warm season (June to August) and cold season (September to May), and against *N2019* over the cold season (September to May) between 2012 and 2014. The upper panel subplots show baseline ELMv1-ECA results (a), and the bottom panel shows updated results from ELMv1a (b). Compared to ELMv1-ECA, large reductions in cold season RMSE of ELMv1a appear over most areas of the whole Alaska domain, especially the NST area.

that the NST ecosystem is a CO_2 source on average from 2012 to 2014 (figure 4(a)). The ELMv1a also estimates an annual CO_2 source for this tundra area, although it is lower by 53.5 gC m^{-2} yr^{-1} compared to *C2017*, mainly due to higher modeled summer CO_2 uptake (figure 3(a)). The annual total difference is smaller (17.1 gC m^{-2} yr^{-1}) for entire Alaska (figure 4(b)), offsetting the larger summer CO_2 uptake by the slightly larger CO_2 emissions from the BF area (figure 3(c)).

Despite the larger summer uptake and thus lower annual emissions, ELMv1a better matched the *C2017* and *N2019* estimates compared to CMIP5 models reported by Commane *et al* (2017b). Specifically, compared to *N2019*, ELMv1a displays smaller differences in September to December total CO_2 emissions (figure 4(c)), i.e. 0.49 TgC yr^{-1} and 3.28 TgC yr^{-1} for ELMv1a and MIROC-ESM-CHEM (i.e. the best CMIP5 model compared to *C2017*), respectively. Indeed, MIROC-ESM-CHEM predicted a 1 month advanced beginning of the growing season compared to *C2017* (Commane *et al* 2017b). In comparison, ELMv1a generally preserves reasonable estimations of peak summer NEE timing.

Compared to *N2019* from 2003 to 2017, ELMv1a simulated slightly smaller total CO_2 emissions during the early cold season (September and October) (figure 5), i.e. −9.1 gC m^{-2} and −1.2 gC m^{-2} on average for NST and Alaska, respectively. The model predicted lower total CO_2 emissions during the cold season with a mean difference of −31.5 gC m^{-2} for the NST, but showed very good agreement for the regional mean over Alaska with a small mean difference of −7.9 gC m^{-2}. The modeled annual CO_2 budget for the NST indicates a net sink of −7.3 gC m^{-2} averagely from 2003 to 2017. Considering the underestimated cold-season total CO_2 emissions compared to *N2019*, however, would alter our conclusion from an annual sink to an annual source (+26.9 gC m^{-2}). Similarly, the modeled SWT is a net sink of −15.7 gC m^{-2} and BF is a net source 8.2 gC m^{-2}, which would be changed to a net source (3.0 gC m^{-2}) and a net sink (−19.6 gC m^{-2}) for SWT and BF, respectively when replacing cold-season estimates with *N2019* (sup. 2). Nonetheless, the spatial variability of CO_2 emissions across Alaska within *N2019* is surprisingly small (figure S1). The large uncertainty in *N2019* (about 0.93 gC m^{-2} d^{-1} for the NS tundra; personal communication with Dr Jennifer Watts) makes the annual CO_2 budget estimate highly elusive.

Overall, despite showing better performance than other CMIP5 model projections, ELMv1a predicts larger summer CO_2 uptake than *C2017* and has smaller cold-season CO_2 emissions compared to *C2017* and *N2019* over the NST. Possible reasons for the

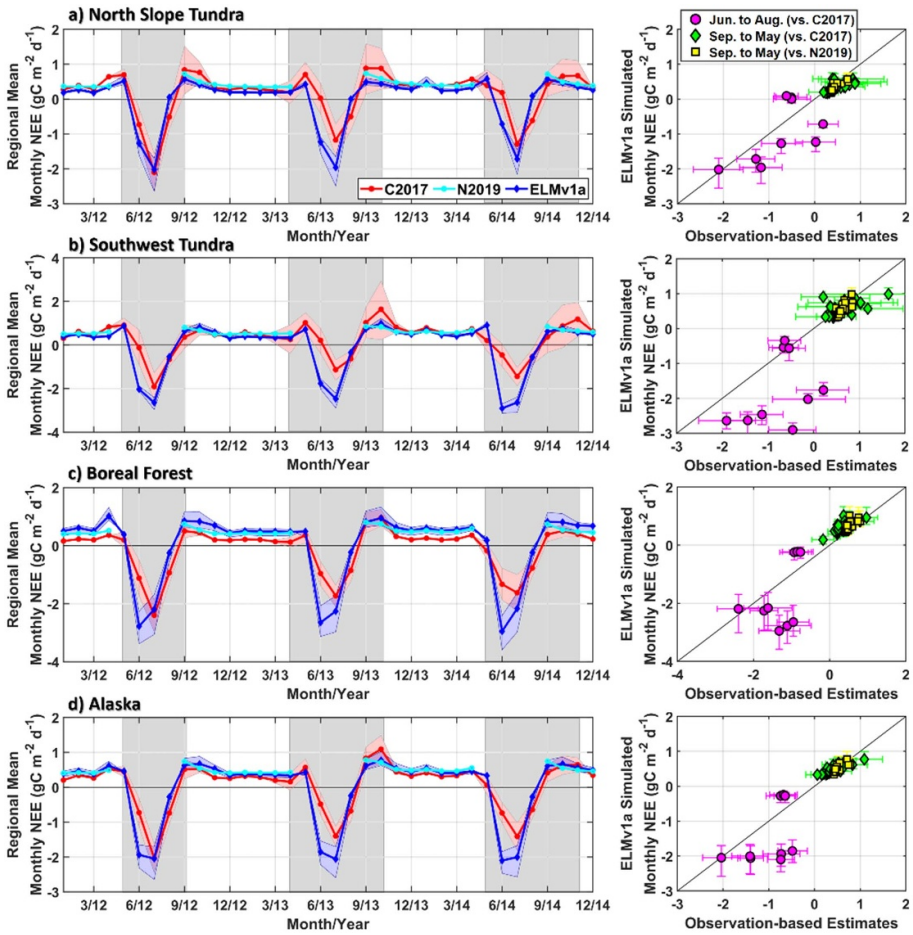

Figure 3. Comparison of ELMv1a-simulated monthly NEE against two observation-constrained estimates (i.e. *C2017* and *N2019*) over three major landcovers and over all of Alaska. The right-hand column subplots are scatter plots contrasting monthly NEE of observation-based estimates against model results, and the symbols are colored by seasonal periods and datasets. '*C2017*' is optimized NEE data with CARVE aircraft measurements (Commane *et al* 2017a). Reddish shaded area indicates the 95% confidence interval (upper and lower bound) of *C2017* estimates. '*N2019*' is a spatial winter NEE dataset derived from ground flux observations with a boosted regression tree machine learning method (Natali *et al* 2019, Watts *et al* 2019). The estimated uncertainty for *N2019* is quite large, e.g. about 0.93 gC m^{-2} d^{-1} (personal communication with Dr Jennifer Watts) for the NST area, and thus is not shown here. Bluish shaded area indicates the model uncertainty associated with representations of temperature sensitivity to HR (section 2.2). Gray background highlight periods when CARVE aircraft measurements were available and used for optimization by *C2017*. Note, since few aircraft measurements were available in the cold season for optimization (supplementary figure S1), the *C2017* estimates of NEE during cold-season months solely come from simulated results (supplementary section sup. 1).

discrepancies between ELMv1a simulations and the observationally-constrained datasets include inaccurate driver and landscape parameters and model deficiencies. Specifically, unresolved grid-cell landscape heterogeneities (particularly in topography, vegetation, and soil properties) impact model estimates of carbon budget via influencing air-vegetation-ground water, carbon, and energy exchanges. The spatial resolution of the reanalysis forcing we used may also be coarser than exists in heterogeneous landscapes. Relevant model deficiencies include: (a) ELMv1a parameterizations for pan-Arctic plant functional types are known to need improvement (Sulman *et al* 2021); (b) ELMv1a lacks representations for dynamic vegetation (e.g. shrub expansion) and ecological disturbances from insects; (c) ELMv1a lacks an appropriate representation for geomorphological disturbances to permafrost landscapes caused by abrupt permafrost thaw and thermokarst formation that release a large amount of permafrost carbon via greenhouse gases (Nitzbon *et al* 2020, Turetsky *et al* 2020); and (d) ELMv1a simulations here did not incorporate the substantial ecosystem disturbance caused by wildfires which also initiate widespread abrupt permafrost thaw and thermokarst development (Holloway *et al* 2020).

3.2. Historical and predicted trends in NEE

The spatial pattern of trends in soil temperature reveals that the largest warming in the top 50 cm soil has occurred in the cold season over the NST (figures 6(a) and (d)). The warming trend of cold-season soil temperature is three times that of the warm-season soil temperature over the NST, i.e.

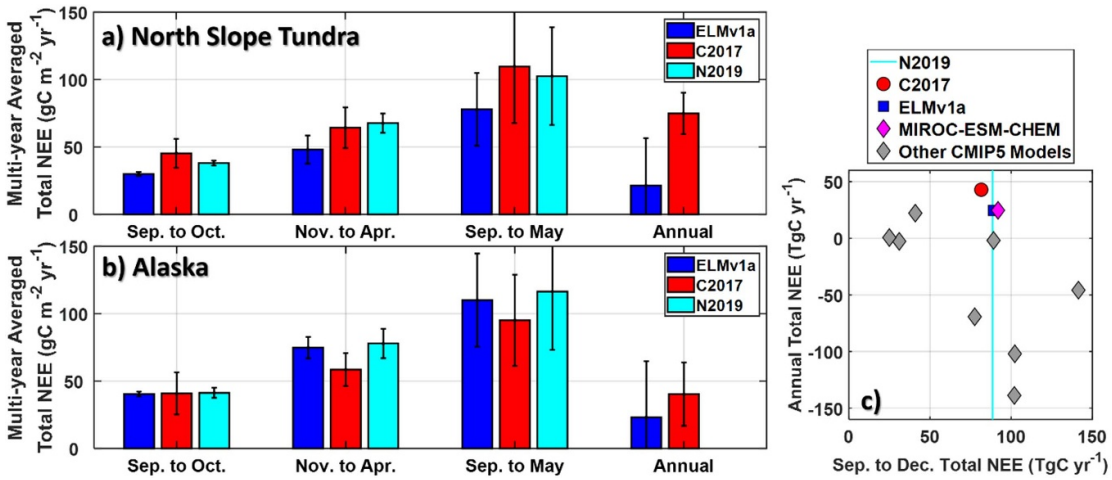

Figure 4. Multi-year (2012–2014) averaged total NEE during different periods (a) over the Alaskan NST and (b) over the whole Alaska domain. Error bars stand for standard deviations. (c) Annual total NEE against September to December total NEE over Alaska. Results of CMIP5 models (including MIROC-ESM-CHEM) were reproduced with permission from Commane *et al* (2017b). Cold season CO_2 emissions simulated by ELMv1a show a good agreement with the two observation-based datasets (i.e. *C2017* and *N2019*), and is among the best results simulated by CMIP5 models (c).

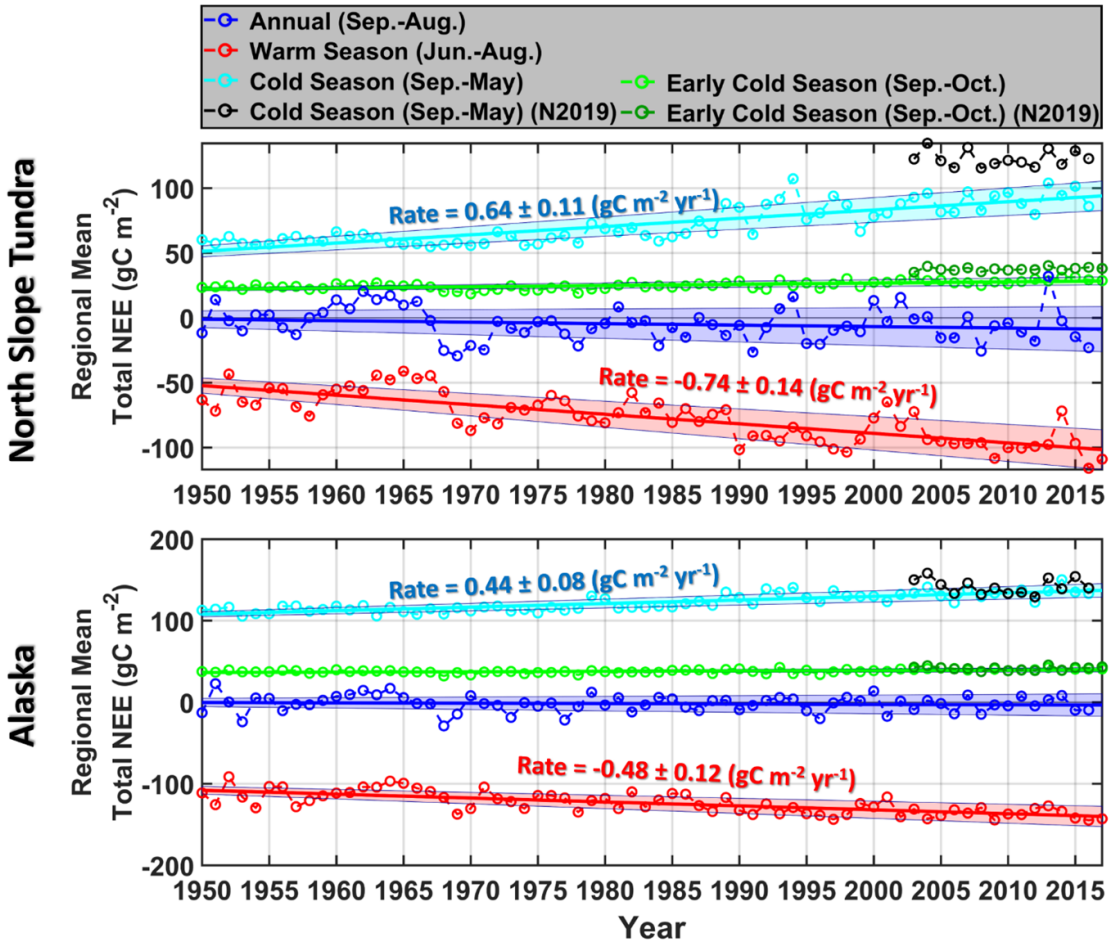

Figure 5. Historical trends (1950–2017) of regionally averaged total NEE over (a) the Alaskan NST area and (b) the whole Alaska domain. The total NEE during the early and entire cold season from *N2019*, an observation-based CO_2 emission dataset derived with a boosted regression tree machine learning method, are also shown. Estimated negative trends of warm-season total NEE (gC m^{-2} yr^{-1}) represent increasing net CO_2 uptake, which outweigh the increasing rates of total cold season CO_2 emissions. Shaded areas indicate the uncertainty bounds (i.e. 95% confidence interval) associated with the estimated trends.

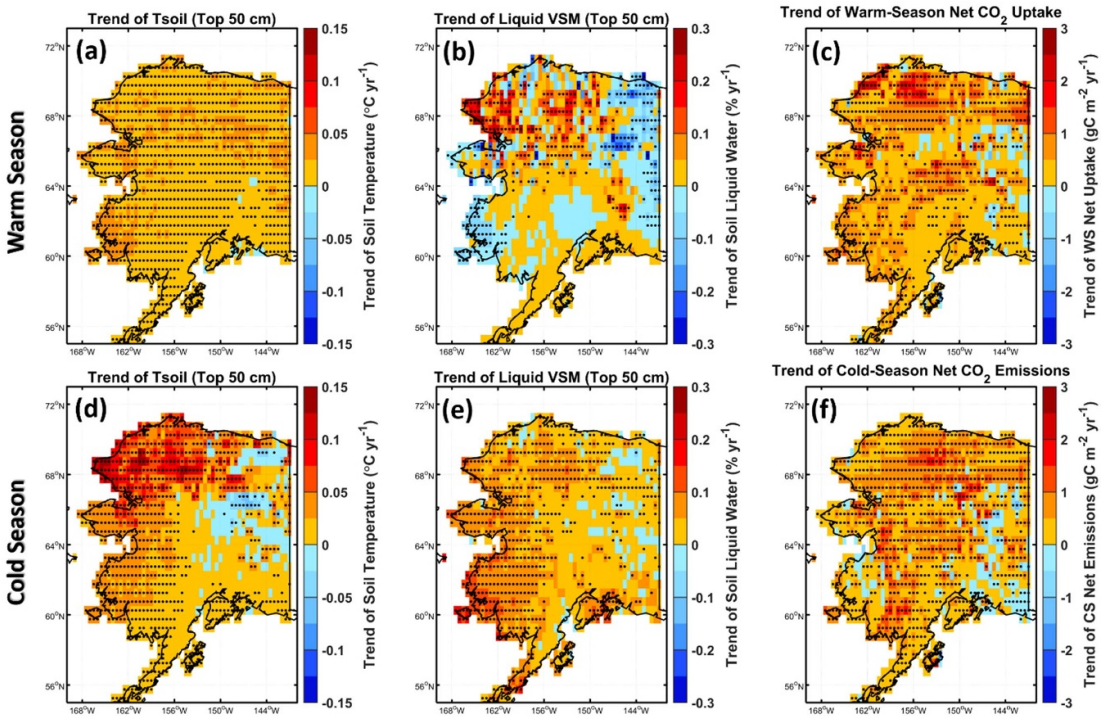

Figure 6. Spatial map of warm season (June to August) and cold season (September to May) trends (1950–2017) in mean soil temperature, liquid VSM, and total net CO_2 uptake or emissions over Alaska. Pixels with a significant trend (p value less than 0.05) are marked by black circles. Both warm-season net CO_2 uptake and cold season net CO_2 emissions show widespread increasing trends. Warming trends in cold-season soil temperature generally are larger than the trends in warm-season soil temperature, especially over the North Slope.

0.06 °C yr^{-1} vs 0.02 °C yr^{-1} (table 1). The map of warm-season trends in top 50 cm liquid volumetric soil moisture (VSM) shows fewer pixels with statistically significant trends (indicated by black circles) than the cold-season map over the NST (figures 6(b) and (e)). The warm-season regional mean VSM over the NST shows the same (but statistically non-significant) increasing rate as for the cold-season (0.04% yr^{-1}; table 1). Both warm-season net ecosystem CO_2 uptake and cold-season net CO_2 emissions show widespread increasing trends over the NST (figures 6(c) and (f)), but showing very different spatial patterns.

Integrated over the NST, we found that warm-season net CO_2 uptake has increased faster than that of cold-season net CO_2 emissions between 1950 and 2017 (figure S6(d) and table 1). Due to recent accelerated warming, the increases in warm-season NEE between 2000 and 2017 were greater than those for the long-term historical periods (i.e. 1950–2017 and 1980–2017) (figure S6(d)), supported by larger increases in warm-season monthly NPP (figure S6(e)) and enhanced plant N and P uptake (figure S7). The increases in HR between 1950 and 2017 were apparently smaller than those between 1980 and 2017 (figure S6(c)), which is attributed to consecutive hydroclimatic disturbances from the late 1960s to early 1970s (Bieniek and Walsh 2017, Sulikowska *et al* 2019), i.e. dry extremes (late 1960s) followed by cold winter extremes (early 1970s) (figure S8). Due to soil moisture and temperature memories of hydroclimatic variabilities, microbial decomposition did not recover to the rate before the hydroclimatic disturbance until several years later (figures S8 and S9). Similar disturbances were also shown for net N and P mineralization (figure S7). In contrast, NPP (figure S6(b)), plant N and P uptake (figures S7 and S8), and leaf C, N and P (figure S10) did not show large reductions during these disturbance periods mainly due to plant nutrient storage and flexible plant stoichiometry for biomass growth (Riley *et al* 2018), demonstrating strong modeled plant resilience to these types of hydroclimatic extremes. In addition, the NST ecosystem sustained productivity under the dry summer extremes (late 1960s) also because of increased WUE (figure S11). However, due to the strong relationship between warm-season NPP and soil temperature (figure S9(e)), cold warm-season extremes would exert a larger impact on plant productivity than HR for a short-term period (e.g. 1998–2000 in figures S8(c.1) and (e.1)).

The climate sensitivity of warm-season net CO_2 uptake, i.e. changes in warm-season cumulative net CO_2 uptake in response to changes in warm-season soil temperature, is 25.1 gC m^{-2} °C^{-1} (figure 7(a)), which is three times greater than the climate sensitivity of cold-season CO_2 emissions (6.8 gC m^{-2} °C^{-1}) (figure 7(b)). The large

Table 1. Historical trend (1950–2017) in regional CO_2 emission, 2 m air temperature, precipitation accumulation, soil temperature and liquid water content in top 50 cm from different periods over the Alaskan NST and Alaska. The negative trend in warm-season total NEE indicates increasing net CO_2 uptake. The uncertainty bounds (i.e. 95% confidence intervals) associated with the estimated trends are indicated in parentheses. (Trends with $p > 0.05$ are not statistically significant and colored grey.)

	NST									
	Total NEE		2 m air temperature		Total precipitation		Top 50 cm mean soil temperature		Top 50 cm mean soil liquid water	
	Trend ($gC\ m^{-2}\ yr^{-1}$)	p value	Trend ($°C\ yr^{-1}$)	p value	Trend ($mm\ yr^{-1}$)	p value	Trend ($°C\ yr^{-1}$)	p value	Trend ($\%\ yr^{-1}$)	p value
Warm season (June–August)	−0.74 (±0.14)	0.00	0.02 (±0.01)	0.00	0.14 (±0.22)	0.21	0.02 (±0.01)	0.00	0.04 (±0.04)	0.06
Early cold season (September–October)	0.10 (±0.03)	0.00	0.03 (±0.02)	0.00	0.10 (±0.09)	0.04	0.02 (±0.01)	0.00	0.06 (±0.04)	0.00
Cold season (September–May)	0.64 (±0.11)	0.00	0.04 (±0.01)	0.00	0.12 (±0.10)	0.02	0.06 (±0.02)	0.00	0.04 (±0.02)	0.00
Annual (September–August)	−0.11 (±0.16)	0.17	0.03 (±0.01)	0.00	0.24 (±0.27)	0.08	0.05 (±0.01)	0.00	0.04 (±0.02)	0.00
	Alaska									
	Total NEE		2 m air temperature		Total precipitation		Top 50 cm mean soil temperature		Top 50 cm mean soil liquid water	
	Trend ($gC\ m^{-2}\ yr^{-1}$)	p value	Trend ($°C\ yr^{-1}$)	p value	Trend ($mm\ yr^{-1}$)	p value	Trend ($°C\ yr^{-1}$)	p value	Trend ($\%\ yr^{-1}$)	p value
Warm season (June–August)	−0.48 (±0.12)	0.00	0.02 (±0.01)	0.00	0.21 (±0.26)	0.11	0.02 (±0.01)	0.00	0.01 (±0.02)	0.46
Early cold season (September–October)	0.05 (±0.02)	0.00	0.02 (±0.01)	0.00	0.13 (±0.21)	0.23	0.01 (±0.01)	0.00	0.03 (±0.02)	0.01
Cold season (September–May)	0.44 (±0.08)	0.00	0.03 (±0.01)	0.00	0.31 (±0.27)	0.02	0.03 (±0.01)	0.00	0.05 (±0.02)	0.00
Annual (September–August)	−0.05 (±0.13)	0.46	0.03 (±0.01)	0.00	0.51 (±0.41)	0.01	0.02 (±0.01)	0.00	0.04 (±0.02)	0.00

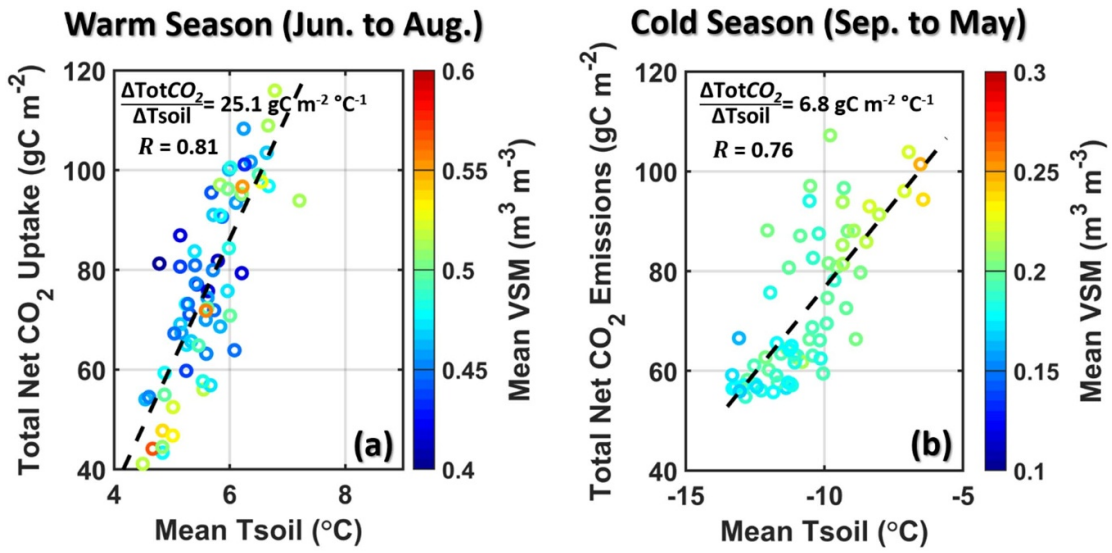

Figure 7. Climate sensitivity of (a) warm season total net CO_2 uptake and (b) cold season total net CO_2 emissions, i.e. the change in warm-season total net uptake (or cold season net emissions) in response to changes in mean soil temperature (top 50 cm) over the NST. Symbols are colored by mean liquid VSM (top 50 cm). The estimated sensitivity $\left(\frac{\Delta \mathrm{TotCO_2}}{\Delta \mathrm{Tsoil}}\right)$ and the correlation coefficients (R) between the time series are included in each panel. Climate sensitivity of warm season net CO_2 uptake is threefold larger than the climate sensitivity of cold-season net emissions in response to the warming climate.

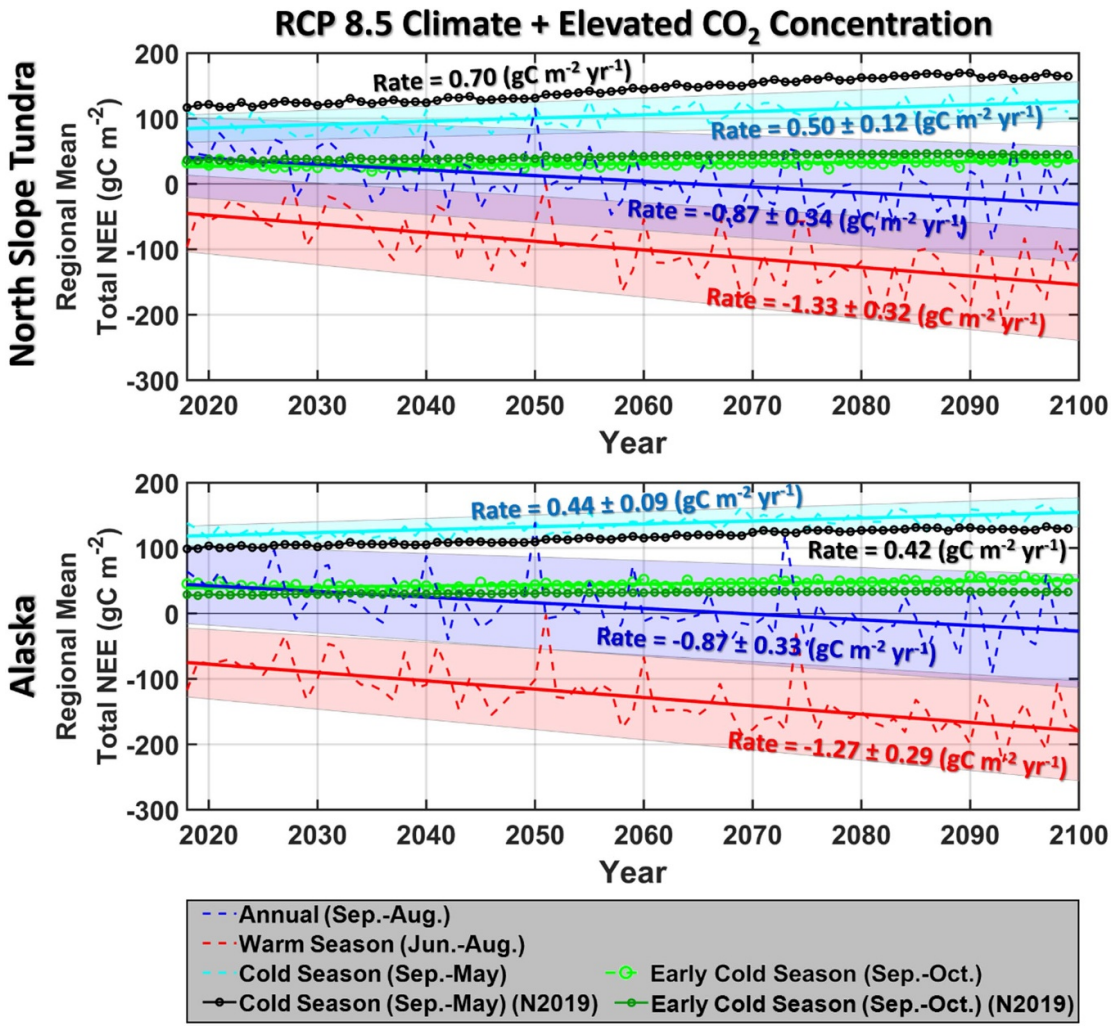

Figure 8. Predicted annual-scale NEE during warm season, early cold season, cold season, and annual cycle over the NST (top) and the whole Alaska domain (bottom) for the RCP8.5_climate + eCO_2 scenario. Estimated trends are included, and shaded areas indicate the associated uncertainty bounds (i.e. 95% confidence interval).

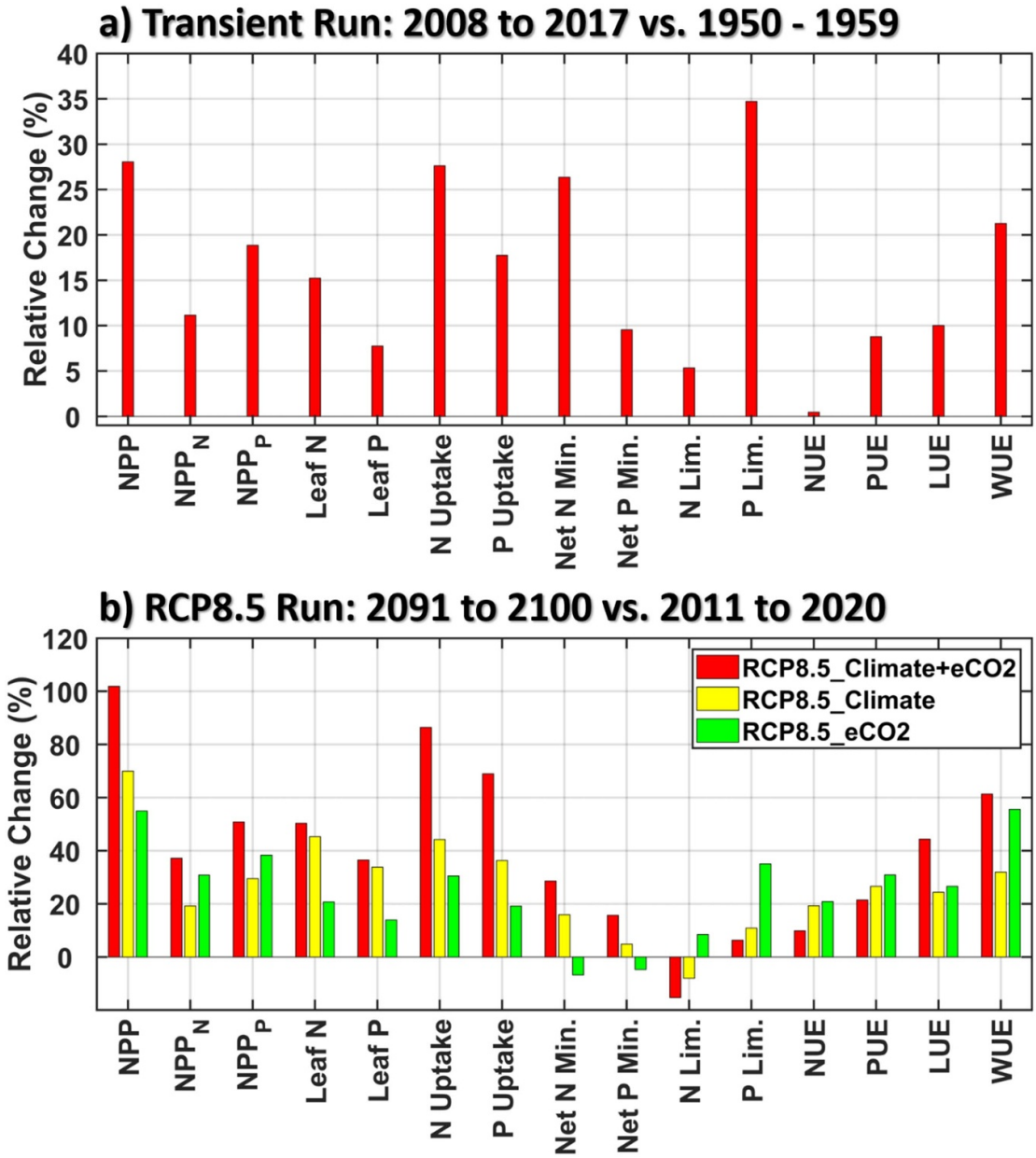

Figure 9. The change of last 10 yr mean relative to the first 10 yr mean for multiple variables including NPP, N- and P-based NPP (NPP_N and NPP_P), leaf N and P, plant N and P uptake, net N and P mineralization, N and P limitation factor, N- and P-use efficiency (NUE and PUE), light- and water-use efficiency (LUE and WUE) for (a) the transient run and (b) three RCP8.5 runs (see details in section 2.2) over the NST.

climate sensitivity of warm-season net CO_2 uptake was reported earlier with tower observations by Yi *et al* (2010). It is mainly caused by enhanced plant productivity due to increased plant N and P uptake and increased LUE and WUE (figures S7–S11). As a result, despite the fact that cold-season soil temperature has warmed three-times as fast as warm-season temperature (table 1), the trend in warm-season net CO_2 uptake is expected to exceed the increasing cold-season CO_2 emissions due to the larger emergent climate sensitivity of warm-season net CO_2 uptake. Indeed, warm-season net CO_2 uptake had a larger increasing trend (0.74 ± 0.14 gC m^{-2} yr^{-1}) than the positive trend for the cold-season total CO_2 emissions (0.64 ± 0.11 gC m^{-2} yr^{-1}) (figure 5 and table 1), leading to a statistically non-significant annual budget trend for the NST between 1950 and 2017 (table 1). The warming climate has increased the first 30 yr (1950–1980) cold-season CO_2 emissions from the NST by 44% (i.e. 86.4 gC m^{-2} vs 60.0 gC m^{-2}) relative to the last 30 yr average (1988–2017), and increased the warm-season net CO_2 uptake by 47% (i.e. 92.3 gC m^{-2} vs 62.7 gC m^{-2}).

With respect to future predictions, the ELMv1a results (RCP8.5_climate + eCO_2) of early cold season CO_2 emissions are similar to those predicted by *N2019* for NST (with a mean difference as −10.9 gC m^{-2}) and Alaska (with a mean difference as 13.3 gC m^{-2}). Under this future scenario, both warm-season net CO_2 uptake and

cold-season CO_2 emissions are projected to continue increasing (figure 8). Compared to the first 30 yr average (2018–2047), the NST cold-season total CO_2 emissions averaged over the last 30 yr (2071–2100) increased by 30% (i.e. 118.4 gC m^{-2} vs 90.8 gC m^{-2}), while warm-season total net CO_2 uptake increased by 108% (i.e. 133.4 gC m^{-2} vs 64.2 gC m^{-2}). Indeed, the increasing rate of warm-season net CO_2 uptake is more than twice that of cold-season CO_2 emissions from 2018 to 2100, i.e. 1.33 ± 0.32 gC m^{-2} yr^{-1} vs 0.50 ± 0.12 gC m^{-2} yr^{-1}, making this critical tundra ecosystem likely a CO_2 sink by 2100, with a significant increasing sink trend at 0.87 $\pm$ 0.34 gC m^{-2} yr^{-1}. However, the model predicted smaller cold-season CO_2 emissions than *N2019* (figure 9) probably because it lacks representations for abrupt permafrost thaw and thermokarst dynamics; and it might also overestimate CO_2 uptake since it does not account for ecosystem disturbances by insects and wildfires. Also, although ELMv1a can simulate dynamics in plant growth and structure (e.g. leaf, stem, roots biomass) via simulating below- and above-ground biomass growth in response to light, water, and nutrient availability, currently it does not represent tundra plant community shifts (e.g. shrub expansion) which might increase CO_2 uptake (Mekonnen *et al* 2018a, 2018b). Representing these disturbances and vegetation community shifts is urgently needed within ESMs to better estimate current and future carbon budgets.

Results showed that enhanced plant N and P uptake and net N and P mineralization support the large CO_2 uptake during the warm season for both the transient (figures 9(a) and S11) and RCP8.5 runs (RCP8.5_climate and RCP8.5_climate + eCO_2) (figures 9 and S12). Although showing positive relative changes in plant productivity for the transient baseline run (figure 9(a)), results indicate potential declines in CO_2 fertilization effects on plant photosynthesis (figure S11) possibly due to nutrient limitations (as also shown by Wang *et al* (2020) for the NST). We evaluated this effect by comparing factorial experiments under the RCP8.5 scenario (section 2.2). Specifically, with the climate fixed at 2011–2020 conditions (RCP8.5_eCO_2), elevated CO_2 first causes large NPP enhancement (figure S13), but then increases in N and P limitation to plant growth from microbial N and P immobilization and decreases in net N and P mineralization (green in figures 9(b) and S13, and the N(P) limitation factor in figure S12). Consequently, the NPP enhancement due to elevated CO_2 is gradually attenuated due to limited N and P availability (RCP8.5_eCO_2 in figure S13). In contrast, the continued warming deepens active layer thickness (figure S14) and thus increases N and P availability, thereby somewhat relieving the N and P limitation, causing negative changes in the N limitation factor (red bar, figure 9(b)) and smaller increases in P limitation (red vs green bars, figure 9(b)). Indeed, both N and P limitation factors first increase and then decrease after their peaks with continued warming (RCP8.5_climate and RCP8.5_climate; red and yellow, figure S12), but persistently increases without climate warming (RCP8.5_eCO_2; green, figure S12). In addition, increased LUE and WUE (figure 9) also contribute to the large trend of warm-season CO_2 net uptake.

4. Summary and conclusions

We used an improved version of the E3SM land model (Tao *et al* 2020: ELMv1a) to investigate warm-season CO_2 net uptake vs cold-season CO_2 net emissions over Alaska under historical and the 21st century RCP8.5 scenario. The model results agree reasonably well with two independent observationally-constrained datasets derived with different methods: using atmospheric measurements and inversion (*C2017*) and using surface-flux measurements and machine learning (*N2019*). Results demonstrate that over the Alaskan NST, although cold-season soil warming was greater than that during the warm-season, the warm-season net CO_2 uptake increased faster (0.74 ± 0.14 gC m^{-2} yr^{-1}) than that of cold-season CO_2 release (0.64 ± 0.11 gC m^{-2} yr^{-1}) between 1950 and 2017. These patterns are held as well for future projections under the RCP8.5 scenario.

The response is attributed to a threefold larger climate sensitivity of warm-season net CO_2 uptake than that of cold-season CO_2 losses. This difference in climate sensitivity is partially (a) due to strong plant resilience to hydroclimatic disturbances, enhanced plant nutrient uptake, increased water- and light-use efficiency, and partially (b) due to weak microbial resilience, i.e. the slow recovery of microbial decomposition rates following consecutive dry summer and cold winter extremes that were built in soil moisture and temperature memories for extended periods. Based on ELMv1a simulations, we therefore conclude that the NST ecosystem will likely remain an annual CO_2 sink through the 21st century. We acknowledge that several factors, including fire, insects, abrupt permafrost thaw, thermokarst dynamics, and landscape-scale hydrological changes that are not discussed here, might alter our conclusion.

Data availability statement

The modeling results that support the findings of this study are available upon reasonable request from the authors.

Acknowledgments

We are grateful for the valuable discussions with Dr Roisin Commane and Dr Jennifer Watts. We thank the anonymous reviewers for their helpful comments.

This material is based upon work supported by the US Department of Energy, Office of Science, Office of Biological and Environmental Research under Award Number DE-SC0019063.

ORCID iD

Jing Tao https://orcid.org/0000-0002-4009-2910

References

Arndt K A, Oechel W C, Goodrich J P, Bailey B A, Kalhori A, Hashemi J, Sweeney C and Zona D 2019 Sensitivity of methane emissions to later soil freezing in arctic tundra ecosystems *J. Geophys. Res.* **124** 2595–609

Ballantyne A *et al* 2017 Accelerating net terrestrial carbon uptake during the warming hiatus due to reduced respiration *Nat. Clim. Change* **7** 148

Belshe E F, Schuur E A G and Bolker B M 2013 Tundra ecosystems observed to be CO_2 sources due to differential amplification of the carbon cycle *Ecol. Lett.* **16** 1307–15

Berner L, Massey R, Jantz P, Forbes B, Macias Fauria M, Myers-Smith I, Kumpula T, Gauthier G, Andreu-Hayles L and Gaglioti B 2020 Summer warming explains widespread but not uniform greening in the Arctic tundra biome *Nat. Commun.* **11** 1–12

Bieniek P A and Walsh J E 2017 Atmospheric circulation patterns associated with monthly and daily temperature and precipitation extremes in Alaska *Int. J. Climatol.* **37** 208–17

Biskaborn B K *et al* 2019 Permafrost is warming at a global scale *Nat. Commun.* **10** 1–11

Bjorkman A D *et al* 2018 Plant functional trait change across a warming tundra biome *Nature* **562** 57

Box J E *et al* 2019 Key indicators of Arctic climate change: 1971−2017 *Environ. Res. Lett.* **14** 045010

Campbell J L and Laudon H 2019 Carbon response to changing winter conditions in northern regions: current understanding and emerging research needs *Environ. Rev.* **27** 545–66

Chen J S, Zhu Q, Riley W J, He Y J, Randerson J T and Trumbore S 2019 Comparison with global soil radiocarbon observations indicates needed carbon cycle improvements in the E3SM land model *J. Geophys. Res.* **124** 1098–114

Cohen J *et al* 2014 Recent Arctic amplification and extreme mid-latitude weather *Nat. Geosci.* **7** 627–37

Cohen J, Pfeiffer K and Francis J A 2018 Warm Arctic episodes linked with increased frequency of extreme winter weather in the United States *Nat. Commun.* **9** 869

Commane R *et al* 2017a CARVE: net ecosystem CO_2 exchange and regional carbon budgets for Alaska, 2012–2014 (https://doi.org/10.3334/ORNLDAAC/1389)

Commane R *et al* 2017b Carbon dioxide sources from Alaska driven by increasing early winter respiration from Arctic tundra *Proc. Natl Acad. Sci. USA* **114** 5361–6

Elmendorf S C *et al* 2012 Plot-scale evidence of tundra vegetation change and links to recent summer warming *Nat. Clim. Change* **2** 453–7

Fahnestock J T, Jones M H, Brooks P D, Walker D A and Welker J M 1998 Winter and early spring CO_2 efflux from tundra communities of northern Alaska *J. Geophys. Res. Atmos.* **103** 29023–7

Fisher J B *et al* 2014 Carbon cycle uncertainty in the Alaskan Arctic *Biogeosciences* **11** 4271–88

Friedlingstein P, Cox P, Betts R, Bopp L, Von Bloh W, Brovkin V, Cadule P, Doney S, Eby M and Fung I 2006 Climate-carbon cycle feedback analysis: results from the C4MIP model intercomparison *J. Clim.* **19** 3337–53

Frost G V, Epstein H E, Walker D A, Matyshak G and Ermokhina K 2013 Patterned-ground facilitates shrub expansion in low Arctic tundra *Environ. Res. Lett.* **8** 015035

Gagnon M, Domine F and Boudreau S 2019 The carbon sink due to shrub growth on Arctic tundra: a case study in a carbon-poor soil in eastern Canada *Environ. Res. Commun.* **1** 091001

Golaz J C *et al* 2019 The DOE E3SM coupled model version 1: overview and evaluation at standard resolution *J. Adv. Model. Earth Syst.* **11** 2089–129

Harris I 2019 CRU JRA v1. 1: a forcings dataset of gridded land surface blend of climatic research unit (CRU) and Japanese reanalysis (JRA) data; January 1901–December 2017 published by: University of East Anglia Climatic Research Unit, Centre for Environmental Data Analysis p 2905

Holloway J E, Lewkowicz A G, Douglas T A, Li X Y, Turetsky M R, Baltzer J L and Jin H J 2020 Impact of wildfire on permafrost landscapes: a review of recent advances and future prospects *Permafrost Periglac* **31** 371–82

Huang J B *et al* 2017 Recently amplified Arctic warming has contributed to a continual global warming trend *Nat. Clim. Change* **7** 875

Hugelius G *et al* 2014 Estimated stocks of circumpolar permafrost carbon with quantified uncertainty ranges and identified data gaps *Biogeosciences* **11** 6573–93

Jeong S J *et al* 2018 Accelerating rates of Arctic carbon cycling revealed by long-term atmospheric CO_2 measurements *Sci. Adv.* **4** eaao1167

Jones M H, Fahnestock J T and Welker J M 1999 Early and late winter CO_2 efflux from Arctic tundra in the Kuparuk river watershed, Alaska, USA *Arct. Antarct. Alp. Res.* **31** 187–90

Kittler F, Heimann M, Kolle O, Zimov N, Zimov S and Gockede M 2017 Long-term drainage reduces CO_2 uptake and CH_4 emissions in a Siberian permafrost ecosystem *Glob. Biogeochem. Cycles* **31** 1704–17

Koenigk T, Brodeau L, Graversen R G, Karlsson J, Svensson G, Tjernstrom M, Willen U and Wyser K 2013 Arctic climate change in 21st century CMIP5 simulations with EC-Earth *Clim. Dyn.* **40** 2719–43

Koven C D, Lawrence D M and Riley W J 2015 Permafrost carbon-climate feedback is sensitive to deep soil carbon decomposability but not deep soil nitrogen dynamics *Proc. Natl Acad. Sci. USA* **112** 3752–7

Koven C D, Ringeval B, Friedlingstein P, Ciais P, Cadule P, Khvorostyanov D, Krinner G and Tarnocai C 2011 Permafrost carbon-climate feedbacks accelerate global warming *Proc. Natl Acad. Sci. USA* **108** 14769–74

Lawrence D M, Slater A G, Romanovsky V E and Nicolsky D J 2008 Sensitivity of a model projection of near-surface permafrost degradation to soil column depth and representation of soil organic matter *J. Geophys. Res. Earth Surf.* **113**

Martin A C, Jeffers E S, Petrokofsky G, Myers-Smith I and Macias-Fauria M 2017 Shrub growth and expansion in the Arctic tundra: an assessment of controlling factors using an evidence-based approach *Environ. Res. Lett.* **12** 085007

McGuire A D *et al* 2012 An assessment of the carbon balance of Arctic tundra: comparisons among observations, process models, and atmospheric inversions *Biogeosciences* **9** 3185–204

Mekonnen Z A, Riley W J and Grant R F 2018a 21st century tundra shrubification could enhance net carbon uptake of North America Arctic tundra under an RCP8.5 climate trajectory *Environ. Res. Lett.* **13** 054029

Mekonnen Z A, Riley W J and Grant R F 2018b Accelerated nutrient cycling and increased light competition will lead to 21st century shrub expansion in North American Arctic tundra *J. Geophys. Res.* **123** 1683–701

Mishra U and Riley W J 2014 Active-layer thickness across Alaska: comparing observation-based estimates with CMIP5 earth system model predictions *Soil Sci. Soc. Am. J.* **78** 894–902

Natali S M *et al* 2019 Large loss of CO_2 in winter observed across the northern permafrost region *Nat. Clim. Change* **9** 852–7

Natali S M, Schuur E A G and Rubin R L 2012 Increased plant productivity in Alaskan tundra as a result of experimental warming of soil and permafrost *J. Ecol.* **100** 488–98

Nitzbon J, Westermann S, Langer M, Martin L C P, Strauss J, Laboor S and BOike J 2020 Fast response of cold ice-rich permafrost in northeast Siberia to a warming climate *Nat. Commun.* **11** 2201

Norby R J, Warren J M, Iversen C M, Medlyn B E and McMurtrie R E 2010 CO_2 enhancement of forest productivity constrained by limited nitrogen availability *Proc. Natl Acad. Sci. USA* **107** 19368–73

Oechel W C, Hastings S J, Vourlitis G, Jenkins M, Riechers G and Grulke N 1993 Recent change of Arctic tundra ecosystems from a net carbon-dioxide sink to a source *Nature* **361** 520–3

Oechel W C, Laskowski C A, Burba G, Gioli B and Kalhori A A M 2014 Annual patterns and budget of CO_2 flux in an Arctic tussock tundra ecosystem *J. Geophys. Res.* **119** 323–39

Oechel W C, Vourlitis G L, Hastings S J, Zulueta R C, Hinzman L and Kane D 2000 Acclimation of ecosystem CO_2 exchange in the Alaskan Arctic in response to decadal climate warming *Nature* **406** 978–81

Outcalt S I, Nelson F E and Hinkel K M 1990 The zero-curtain effect—heat and mass-transfer across an isothermal region in freezing soil *Water Resour. Res.* **26** 1509–16

Parazoo N C, Commane R, Wofsy S C, Koven C D, Sweeney C, Lawrence D M, Lindaas J, Chang R Y W and Miller C E 2016 Detecting regional patterns of changing CO_2 flux in Alaska *Proc. Natl Acad. Sci. USA* **113** 7733–8

Parazoo N C, Koven C D, Lawrence D M, Romanovsky V and Miller C E 2018 Detecting the permafrost carbon feedback: talik formation and increased cold-season respiration as precursors to sink-to-source transitions *Cryosphere* **12** 123–44

Piao S L *et al* 2008 Net carbon dioxide losses of northern ecosystems in response to autumn warming *Nature* **451** 49–U43

Pithan F and Mauritsen T 2014 Arctic amplification dominated by temperature feedbacks in contemporary climate models *Nat. Geosci.* **7** 181–4

Qian H F, Joseph R and Zeng N 2010 Enhanced terrestrial carbon uptake in the northern high latitudes in the 21st century from the coupled carbon cycle climate model intercomparison project model projections *Glob. Change Biol.* **16** 641–56

Riley W J, Zhu Q and Tang J Y 2018 Weaker land-climate feedbacks from nutrient uptake during photosynthesis-inactive periods *Nat. Clim. Change* **8** 1002

Rustad L E, Campbell J L, Marion G M, Norby R J, Mitchell M J, Hartley A E, Cornelissen J H C and Gurevitch J 2001 Gcte-news: a meta-analysis of the response of soil respiration, net nitrogen mineralization, and aboveground plant growth to experimental ecosystem warming *Oecologia* **126** 543–62

Schaefer K, Lantuit H, Romanovsky V E, Schuur E A G and Witt R 2014 The impact of the permafrost carbon feedback on global climate *Environ. Res. Lett.* **9** 085003

Schuur E A G *et al* 2015 Climate change and the permafrost carbon feedback *Nature* **520** 171–9

Sturm M, Schimel J, Michaelson G, Welker J M, Oberbauer S F, Liston G E, Fahnestock J and Romanovsky V E 2005 Winter biological processes could help convert Arctic tundra to shrubland *Bioscience* **55** 17–26

Sulikowska A, Walawender J P and Walawender E 2019 Temperature extremes in Alaska: temporal variability and circulation background *Theor. Appl. Climatol.* **136** 955–70

Sulman B N, Salmon V G, Iversen C M, Breen A L, Yuan F and Thornton P E 2021 Integrating Arctic plant functional types in a land surface model using above-and belowground field observations *J. Adv. Model. Earth Syst.* **13**

Tao J, Zhu Q, Riley W J and Neumann R B 2020 Improved ELMv1-ECA simulations of zero-curtain periods and cold-season CH_4 and CO_2 emissions at Alaskan Arctic tundra sites *Cryosphere Discuss.* **2020** 1–48

Trucco C, Schuur E A G, Natali S M, Belshe E F, Bracho R and Vogel J 2012 Seven-year trends of CO_2 exchange in a tundra ecosystem affected by long-term permafrost thaw *J. Geophys. Res.* **117** G02031

Turetsky M R *et al* 2020 Carbon release through abrupt permafrost thaw *Nat. Geosci.* **13** 138

Waelbroeck C, Monfray P, Oechel W C, Hastings S and Vourlitis G 1997 The impact of permafrost thawing on the carbon dynamics of tundra *Geophys. Res. Lett.* **24** 229–32

Wang S H *et al* 2020 Recent global decline of CO_2 fertilization effects on vegetation photosynthesis *Science* **370** 1295

Wang Y H *et al* 2019 Mechanistic modeling of microtopographic impacts on CO_2 and CH_4 fluxes in an Alaskan tundra ecosystem using the CLM-microbe model *J. Adv. Model. Earth Syst.* **11** 4288–304

Watts J D, Natali S, Potter S and Rogers B M 2019 Gridded winter soil CO_2 flux estimates for pan-Arctic and boreal regions 2003–100

Yi C X *et al* 2010 Climate control of terrestrial carbon exchange across biomes and continents *Environ. Res. Lett.* **5** 034007

Zaehle S *et al* 2014 Evaluation of 11 terrestrial carbon-nitrogen cycle models against observations from two temperate free-air CO_2 enrichment studies *New Phytol.* **202** 803–22

Zhang W X, Miller P A, Smith B, Wania R, Koenigk T and Doscher R 2013 Tundra shrubification and tree-line advance amplify Arctic climate warming: results from an individual-based dynamic vegetation model *Environ. Res. Lett.* **8** 034023

Zhang W, Jansson C, Miller P A, Smith B and Samuelsson P 2014 Biogeophysical feedbacks enhance the Arctic terrestrial carbon sink in regional Earth system dynamics *Biogeosciences* **11** 5503–19

Zhu Q, Riley W J, Iversen C M and Kattge J 2020 Assessing impacts of plant stoichiometric traits on terrestrial ecosystem carbon accumulation using the E3SM land model *J. Adv. Model. Earth Syst.* **12** e2019MS001841

Zhu Q, Riley W J, Tang J Y, Collier N, Hoffman F M, Yang X J and Bisht G 2019 Representing nitrogen, phosphorus, and carbon interactions in the E3SM land model: development and global benchmarking *J. Adv. Model. Earth Syst.* **11** 2238–58

Zona D, Gioli B, Commane R, Lindaas J, Wofsy S C, Miller C E, Dinardo S J, Dengel S, Sweeney C and Karion A 2016 Cold season emissions dominate the Arctic tundra methane budget *Proc. Natl Acad. Sci.* **113** 40–5